

Tracing the star formation history of cluster galaxies using the $H\alpha/UV$ flux ratio

J. Iglesias-Páramo¹, A. Boselli¹, G. Gavazzi², and Antonio Zaccardo²

¹ Laboratoire d'Astrophysique de Marseille, Traverse du Siphon - Les Trois Lucs, 13376 Marseille, FRANCE
e-mail: jorge.iglesias@oamp.fr, alessandro.boselli@oamp.fr

² Università degli Studi di Milano - Bicocca, P.zza delle scienze 3, 20126 Milano, Italy.
e-mail: giuseppe.gavazzi@mib.infn.it, antonio.zaccardo@mib.infn.it

Received ...; accepted ...

Abstract. Since the $H\alpha$ and UV fluxes from galaxies are sensitive to stellar populations of ages $< 10^7$ and $\approx 10^8$ yr respectively, their ratio $f(H\alpha)/f(UV)$ provides us with a tool to study the recent $t \leq 10^8$ yr star formation history of galaxies, an exercise that we present here applied to 98 galaxies in 4 nearby clusters (Virgo, Coma, Abell 1367 and Cancer). The observed $f(H\alpha)/f(UV)$ ratio is \sim a factor of two smaller than the expected one as determined from population synthesis models assuming a realistic delayed, exponentially declining star formation history. We discuss various mechanisms that may have affected the observed $f(H\alpha)/f(UV)$ ratio and we propose that the above discrepancy arises from either the absorption of Lyman continuum photons by dust within the star formation regions or from the occurrence of star formation episodes. After splitting our sample into different subsamples according to evolutionary criteria we find that our reference sample of galaxies unaffected by the cluster environment show an average value of $f(H\alpha)/f(UV)$ two times lower than the expected one. We argue that this difference must be mostly due to absorption of $\approx 45\%$ of the Lyman continuum photons within star forming regions. Galaxies with clear signs of an ongoing interaction show average values of $f(H\alpha)/f(UV)$ slightly higher than the reference value, as expected if those objects had SFR increased by a factor of $\simeq 4$. The accuracy of the current UV and $H\alpha$ photometry is not yet sufficient to clearly disentangle the effect of interactions on the $f(H\alpha)/f(UV)$ ratio, but significant observational improvements are shortly expected to result from the GALEX mission.

Key words. galaxies: star formation – galaxies: clusters

1. Introduction

A number of environmental mechanisms able of affecting significantly the evolution of galaxies in rich clusters have been proposed in the literature: gas stripping by ram pressure (Gunn & Gott 1972; Abadi, Moore & Bower 1999), galaxy-galaxy harassment in close encounters (Moore et al. 1996), tidal stirring by the cluster potential (Byrd & Valtonen 1990; Fujita 1998).

These mechanisms should produce morphological disturbances, gas removal and, on long timescales, significant quenching of the star formation rates (SFRs) of galaxies due to “fuel” exhaustion (see Gavazzi et al. 2002a). However galaxy-galaxy interactions might also enhance the star formation in gas-rich systems, both in their nuclei and disks, as it has been observed at several wavelengths (Larson & Tinsley 1978; Kennicutt et al. 1987; Hummel et al. 1987; Soifer et al. 1984), although this **enhancement** might be mild (Bergvall et al. 2003). The dynamical in-

teraction of galaxies with the IGM can also produce an enhancement in the galaxies SFR by ram pressure (Fujita & Nagashima 1999).

A conclusive evidence for a separate evolution of galaxies in clusters is offered by the Butcher-Oemler effect (Butcher & Oemler 1978), i.e. distant ($z \sim 0.3$) clusters show a larger fraction of blue galaxies than nearby clusters. Several follow-up studies (Couch & Sharples 1987; Barger et al. 1996; Couch et al. 1994; Poggianti et al. 1999; Balogh et al. 1999) brought to today’s accepted scenario that clusters are continuously accreting galaxies from their neighborhood, with the accretion rate increasing with look-back time.

Several observable quantities have been proposed as reliable estimators of the SFRs of galaxies (Kennicutt 1998; Rosa-González et al. 2002): $H\alpha$, UV, radio continuum and Far-IR luminosities. Among these, we focus our analysis on the $H\alpha$ and UV luminosities. The $H\alpha$ luminosity comes from stars more massive than $10M_{\odot}$ and it traces the SFR in the last $\leq 10^7$ yr. The UV luminosity at 2000 \AA comes

from stars more massive than $1.5M_{\odot}$ and it can be used as an indicator of the SFR in the last $\approx 10^8$ yr, under the condition that it stayed approximately constant during this period. The two quantities combined, in other words the ratio $f(\text{H}\alpha)/f(\text{UV})$, should give us a “clock” suitable for telling if the SFR was constant over the last 10^8 yr.

The present paper is aimed at studying the role of the cluster environment on the star formation histories of cluster galaxies by using the $f(\text{H}\alpha)/f(\text{UV})$ ratio for a sample of galaxies in four nearby clusters: Virgo, Coma, Abell 1367 and Cancer. This analysis relies on the multifrequency database that we collected so far for a large sample of galaxies in nearby cluster and we made available to the community through the GOLDmine WEB site (Gavazzi et al. 2003). Beside the H α and UV data which are directly used for computing the two SFR indicators, other corollary data (e.g. Near-IR, Far-IR, HI fluxes and optical spectroscopy) are used throughout this paper. These corollary data play a fundamental role in the determination of the dust extinction at UV wavelengths (through the FIR/UV ratio, e.g. Buat & Xu 1996) and at H α (from the Balmer decrement, e.g. Lequeux et al. 1981).

The galaxy sample is presented in Section 2. The observed vs. expected $f(\text{H}\alpha)/f(\text{UV})$ ratio for cluster galaxies is discussed in Section 3. In Section 4 we discuss the limitations and the potentiality of the method applied in this preliminary analysis. A brief summary of the results is presented in Section 5. Details about the estimate of the birthrate parameter b are given in Appendix A. A second appendix contains a detailed analysis of the observational uncertainty affecting the $f(\text{H}\alpha)/f(\text{UV})$ ratio.

2. The sample of cluster galaxies

The sample analyzed in this work includes late-type galaxies (morphological type later than Sa) belonging to four nearby clusters: Virgo, Coma, A1367 and Cancer. Among Virgo galaxies we selected all objects in the Virgo Cluster Catalogue (VCC, Binggeli et al. 1985 with $m_{\text{pg}} \leq 18$) and for Coma, A1367 and Cancer all galaxies in the Zwicky Catalogue (CGCG, Zwicky et al. 1961-1968 with $m_{\text{pg}} \leq 15.7$). The accuracy of the morphological classification is excellent for the Virgo galaxies (Binggeli et al. 1985; 1993). Because of the larger distances, the morphology of galaxies belonging to the other surveyed regions suffers from an uncertainty of about 1.5 Hubble type bins. We assume a distance of 17 Mpc for the members (and possible members) of Virgo cluster A, 22 Mpc for Virgo cluster B, 32 Mpc for objects in the M and W clouds (see Gavazzi et al. 1999). Members of the Cancer, Coma and A1367 clusters are assumed at distances of 62.6, 86.6 and 92 Mpc respectively. Isolated galaxies in the Coma supercluster are assumed at their redshift distance adopting $H_0 = 75 \text{ km s}^{-1} \text{ Mpc}^{-1}$.

2.1. The observational dataset

The photometric and spectroscopic data necessary for carrying out the present analysis (taken from the GOLDmine database: <http://goldmine.mib.infn.it/>; Gavazzi et al. 2003) are the following:

1. H α fluxes, necessary to determine the present ($\leq 10^7$ years), massive SFR (Kennicutt 1998). H α + [NII] fluxes have been obtained from imaging (Iglesias-Páramo et al. 2002; Boselli & Gavazzi 2002; Boselli et al. 2002; Gavazzi et al. 2002b, and references therein): they are integrated values and, contrary to many other samples used for similar analysis, they do not suffer from aperture biases. The estimated error on the H α + [NII] flux is $\sim 15\%$.
2. UV (2000 Å) fluxes, useful to compute the intermediate age ($\leq 3 \times 10^8$ years) star formation activity (Buat et al. 1987). The UV data are taken from the FAUST (Lampton et al. 1990) and the FOCA (Milliard et al. 1991) experiments. For the sake of consistency with our previous works, we transformed UV magnitudes taken at 1650 Å by Deharveng et al. (1994) to 2000 Å assuming a constant colour index $m_{2000} = m_{1650} + 0.2$ mag (see Boselli et al. 2003). These are total magnitudes, determined by integrating the UV emission down to the weakest detectable isophote. The estimated error on the UV magnitude is 0.3 mag in general, but it ranges from 0.2 mag for bright galaxies to 0.5 mag for weak sources observed in frames with larger than average calibration uncertainties.
3. Far-IR (60, 100 μm) fluxes, for obtaining an accurate UV extinction correction (Buat et al. 2002; Boselli et al. 2003). Far-IR at 60 and 100 μm integrated flux densities from the IRAS survey are taken mainly from the IRAS FSC (Moshir et al. 1989). Three galaxies are not detected at one of these two IRAS bands and an upper limit is estimated to the flux: VCC 1725, CGCG 119-053 and CGCG 097-062. In addition, no IRAS data are available for VCC 1699; instead, ISO data were used for this galaxy. The conversion between the ISO and IRAS fluxes was taken from Boselli et al. (2003). Typical uncertainties on the Far-IR data are $\sim 15\%$.
4. Long slit integrated spectroscopy with detected H α and H β lines, necessary for the determination of the Balmer decrement. Long slit, drift-scan mode spectra were obtained by (Gavazzi et al. 2003b) by drifting the slit over the whole galaxy disk, as in Kennicutt (1992). These are intermediate ($\lambda/\Delta\lambda \sim 1000$) resolution spectra in the range (3600 – 7200 Å). The accuracy on the determination of the line intensities is $\approx 10\%$ for H α and H β and $\approx 15\%$ for [NII] $\lambda\lambda 6548, 6584\text{Å}$.

Due to these strong observational constraints the final sample is restricted to 98 galaxies. Because of the above selection criteria, and in particular owing to the condition that galaxies must be detected in H β , our sample might

be affected by observational biases that will be discussed in a subsequent section.

Further corollary data, when available, are used to provide information on the evolutionary state of the sample galaxies:

1. In order to quantify the degree of perturbation by the cluster-IGM, we use the HI deficiency parameter, defined as the logarithm of the ratio of the observed HI mass to the average HI mass of isolated objects of similar morphological type and linear size (Haynes & Giovanelli 1984). Galaxies with $def(\text{HI}) < 0.4$ are considered as unperturbed objects.
2. The asymmetry of the HI profile of the individual galaxies was also included in our analysis as an indicator of interactions in the last $\simeq 10^8$ yr, as done in Gavazzi (1989). A galaxy with a line of sight inclination $> 30^\circ$ is considered asymmetric in HI if its profile deviates significantly from the expected two-horns profile typical of unperturbed inclined galaxies, i.e. if the peak of the lowest horn is smaller than 50 % that of the highest one. By definition, this indicator is meaningless for face-on galaxies where the profile is a single horn. HI profiles were taken from Giovanelli & Haynes (1985), Bothun et al. (1985), Chincarini et al. (1983), Helou et al. (1984), Gavazzi (1989), Haynes & Giovanelli (1986), Hoffman et al. (1989), Schneider et al. (1990) and Bravo-Alfaro et al. (2001).
3. Near-IR total H -band magnitudes are derived consistently with Gavazzi & Boselli (1996) for most of the galaxies, with an accuracy of 10%. For galaxies VCC 318, 459, 664, 971, 1189, 1575, 1678, 1699 and 1929, with no H -band magnitude available, it was derived from the K -band magnitude adopting $(H - K) = 0.25$ on average. The H -band magnitude for VCC 552 and 1091 was taken from the 2MASS All-Sky Extended Source Catalog (XSC).

H -band luminosities are required, together with the H α ones, to estimate the birthrate parameter, b , defined as (Kennicutt et al. 1994):

$$b = \frac{\text{SFR}(t)}{\langle \text{SFR}(t') \rangle} \quad (1)$$

where $\text{SFR}(t)$ is the SFR at the present epoch and $\langle \text{SFR}(t') \rangle$ is the average SFR over the galaxy lifetime. If we model the SF history of normal galaxies with a delayed exponential law, called “a la Sandage” (Gavazzi et al. 2002a), a value of the birthrate parameter b_{model} can be estimated. On the other hand, an observational value of the birthrate parameter b_{obs} can be obtained from the H α and H -band luminosities (see Boselli et al. 2001 and Appendix A for details about the calculation of b_{model} and b_{obs}). As the cluster environment can alter the galaxies’ SFH, the ratio $b_{\text{obs}}/b_{\text{model}}$ should reflect the deviation of the real SFH from the analytical one, and thus it should provide us with an estimate of the effect of the environment on cluster galaxies.

The basic quantities used in this analysis are listed in Table 1, arranged as follows:

Col. (1): Galaxy name.

Col. (2): log of the H α flux corrected for dust extinction and [NII] contamination as described in Section 2.2.1., in $\text{erg s}^{-1} \text{cm}^{-2}$.

Col. (3): log of the UV flux corrected for extinction as described in Section 2.2.2., in $\text{erg s}^{-1} \text{cm}^{-2} \text{\AA}^{-1}$.

Col. (4): log of the H -band luminosity.

Col. (5): HI deficiency parameter.

Col. (6): Asymmetry of the HI profile: “S” = symmetric, “A” = asymmetric and “?” = unclassified HI profile.

2.2. Extinction Correction

2.2.1. H α + [NII] fluxes

H α + [NII] fluxes have been corrected for dust extinction and [NII] contamination as in Buat et al. (2002). The integrated spectra, available for all galaxies, have been used to estimate the H α /[NII] line ratio and the Balmer decrement. On all spectra we were able to measure the underlying Balmer absorption at H β . This measurement is absolutely necessary for an accurate determination of the Balmer decrement in intermediate star forming galaxies, where the underlying absorption is comparable to the emission line. The average H β equivalent width in absorption in our sample is 4.75 \AA .

Despite the fact that the two [NII] forbidden lines are close to H α , the triplet was successfully deblended in most cases by fitting three gaussian components to the ensemble of the three lines or taking advantage of the fact that the ratio [NII] $\lambda 6548/\lambda 6584$ is approximately constant. For those galaxies for which the [NII] $\lambda 6548$ \AA emission line was not detected, we used the theoretical relationship [NII] $\lambda 6548 + \lambda 6584$ $\text{\AA} = 1.33 \times$ [NII] $\lambda 6584$ \AA (Osterbrock 1989).

Given the proximity of the [NII] doublet, deblending the underlying Balmer absorption at H α results impossible. Since on average the equivalent width in absorption at H α is expected similar to within few percent to that of the H β (see Charlot & Longhetti 2001 and references therein) its inclusion should result in a negligible correction to the relatively strong H α line. Therefore no correction for underlying absorption at H α was applied.

2.2.2. UV fluxes

UV fluxes have been corrected for galactic extinction according to Burstein & Heiles (1982) and for internal extinction assuming the recipe of Boselli et al. (2003), based on the Far-IR to UV flux ratio. This correction is, at present, the most accurate and less model dependent, being mostly independent on the geometry, on the SFH of galaxies and on the assumed extinction law.

For the three galaxies with available fluxes at only one of the IRAS bands (60 or 100 μm), the flux in the undetected IRAS band was estimated using the templates

SED of galaxies of similar luminosity given in Boselli et al. (2003).

3. The H α /UV ratio of star forming galaxies

Gavazzi et al. (2002a) showed that the time evolution of optically selected galaxies of the Virgo cluster can be reproduced assuming an universal IMF (Salpeter) and a SFH “a la Sandage”. This form represents a “delayed exponential” SFH whose analytical representation as a function of time t (where t is the age of the galaxy) is:

$$\text{SFR}(t, \tau) \propto (t/\tau)^2 e^{-t^2/2\tau^2} \quad (2)$$

As described in Gavazzi et al. (2002a; see their fig. 5), the temporal evolution of this family of functions is a delayed rise of the SFR up to a maximum (at $t = \sqrt{2}\tau$), followed by an exponential decrease. Both the delay time and the steepness of the decay are regulated by a single parameter τ .

The parameter τ was found to scale with the H -band luminosity, or in other words that the SFR of galaxies at a given time is determined by its H -band luminosity. The values of τ found for our sample galaxies range from $3.5 \leq \tau \leq 8.5$ Gyr for normal spirals and $\tau \geq 8.5$ for star forming dwarf galaxies of types Im and BCDs.

For any galaxy whose spectral energy distribution (SED) is known, the knowledge of SFR(t) allows to predict the expected value (at any time t) of any observable quantity A once we know its time evolution by integrating over the lifetime of the galaxy:

$$A_{\text{exp}}(t) = \int_0^t \text{SFR}(t', \tau) A(t' - t) dt' \quad (3)$$

where $A_{\text{exp}}(t)$ is the expected value of the variable A at time t and $t = 0$ corresponds to the epoch of galaxy formation.

Assuming eq. 2 for the SFH, we show in fig. 1 the time evolution of the $f(\text{H}\alpha)/f(\text{UV})$ ratio for different values of τ . The Starburst99 (Leitherer et al. 1999) code was used, assuming a Salpeter IMF and solar metallicity. As the plot shows, the ratio $f(\text{H}\alpha)/f(\text{UV})$ shows a steep decrease in the first 1 Gyr of evolution for any τ . Between 1 and 13 Gyr the ratio $f(\text{H}\alpha)/f(\text{UV})$ continues to decrease for $\tau = 1$ Gyr which is typical of the brightest elliptical galaxies (see Gavazzi et al. 2002a). For $\tau \geq 3$ Gyr, appropriate for normal spirals and star forming dwarfs such as those analyzed in our work, the ratio $f(\text{H}\alpha)/f(\text{UV})$ remains almost constant for $t \geq 10^9$ yr. Thus, if spiral galaxies follow a time evolution “a la Sandage” as in eq. 2 (i.e., an almost constant SFR over the last $\approx 10^8$ yr), we expect $\log f(\text{H}\alpha)/f(\text{UV}) \approx 1.43$ at the present time, according to the Starburst99 code and assuming solar metallicity and a Salpeter IMF between 0.1 and $100M_{\odot}$. A good agreement with this value is found when comparing the stability of this result to previous values reported in the literature assuming realistic SFHs and similar IMFs and metallicities – 1.37 (Kennicutt et al. 1998), 1.42 (Madau et al. (1998)

and 1.51 (Boselli et al. 2001) – so, it will be used as the reference value in the subsequent analysis.

The histogram of the observed $f(\text{H}\alpha)/f(\text{UV})$ ratio for our sample galaxies in fig. 2 shows an almost symmetric distribution centered at $\log f(\text{H}\alpha)/f(\text{UV}) = 1.17$ ($\sigma = 0.25$ dex), significantly lower than the expected value for a SFH “a la Sandage” ($\log f(\text{H}\alpha)/f(\text{UV}) = 1.43$, indicated by the dashed line in the plot).

The dispersion of the $f(\text{H}\alpha)/f(\text{UV})$ distribution is consistent with that expected from the observational uncertainties, as shown in Appendix B. The systematic difference between the average observed value and the model prediction (0.27 dex) can hardly be explained by systematic errors in the calibration of the data and of the models. The nature of this difference, which we believe real, is discussed in what follows.

3.1. Variable IMF

The $f(\text{H}\alpha)/f(\text{UV})$ ratio depends on the assumed IMF. Changing the slope and M_{up} of the IMF results in changes in the relative numbers of the high-to-low mass stars as summarized in Table 2. This table shows, for instance, the dependence of the $f(\text{H}\alpha)/f(\text{UV})$ ratio on the IMF, assuming instantaneous bursts and constant star formation during 10^6 , 10^7 and 10^8 yr (Starburst99 models). Three IMFs were chosen: Salpeter ($\alpha = -2.35$ and $M_{\text{up}} = 100M_{\odot}$), truncated Salpeter ($\alpha = -2.35$ and $M_{\text{up}} = 30M_{\odot}$), and Miller-Scalo ($\alpha = -3.30$ and $M_{\text{up}} = 100M_{\odot}$; Miller & Scalo 1979). Not unexpectedly the Salpeter IMF gives the highest $f(\text{H}\alpha)/f(\text{UV})$ ratio, since it corresponds to the highest high-to-low mass stars fraction. Changing the IMF produces changes of $f(\text{H}\alpha)/f(\text{UV})$ of the order of ± 0.25 dex for the constant SFR case. These results are quite stable against the use of different population synthesis models: using similar initial conditions, Starburst99 yields values of $f(\text{H}\alpha)/f(\text{UV}) \approx 0.07$ dex larger than PEGASE2.

From the observational point of view there is no compelling evidence for a non universal IMF in galaxies. The lack of any relationship between the $f(\text{H}\alpha)/f(\text{UV})$ ratio and the morphological type or luminosity, as shown in fig. 3, justifies the use of the same IMF for all classes of galaxies. Moreover several studies indicate that the Salpeter IMF for $M_* \geq 3M_{\odot}$ is adequate for several nearby galaxies and for the Galaxy (Sakhibov & Smirnov 2000; Massey 1998; Massey & Hunter 1998; see however Figer et al. 1999; Eisenhauer et al. 1998).

3.2. Variable metallicity

The $f(\text{H}\alpha)/f(\text{UV})$ ratio also depends on the metallicity of galaxies, as shown in Table 2. The dispersion due to metallicity is maximum for an instantaneous burst and it decreases in the case of constant star formation over the last 10^8 yr. The contribution of metallicity to the dispersion of the $f(\text{H}\alpha)/f(\text{UV})$ distribution should be however

minor since the metallicities of our sample galaxies range from Z_{\odot} to $0.1Z_{\odot}$ (see Gavazzi et al. 2002a). We expect the dispersion of the $f(\text{H}\alpha)/f(\text{UV})$ distribution due to metallicity to be ± 0.04 dex around the mean theoretical value of $\log f(\text{H}\alpha)/f(\text{UV})$, this result being independent on the adopted populations synthesis model. Thus, the systematic difference between the observed $f(\text{H}\alpha)/f(\text{UV})$ distribution and the theoretical value can hardly be ascribed to the different metallicities of the sample galaxies.

3.3. Escaping of Lyman continuum photons

A non negligible fraction of the Lyman continuum photons can escape galaxies without ionizing hydrogen atoms. This effect would produce an overall shift of the $f(\text{H}\alpha)/f(\text{UV})$ distribution towards lower values. Indirect estimates of the escape fraction of Lyman continuum photons from HII regions determined from the ionization of the diffuse gas by Zurita et al. (2000) led to values of $\sim 50\%$ in spiral discs. **However, as pointed out by these authors, this has to be taken as an upper limit to the photons which escape from the galaxy since many of these ionizing photons will be absorbed by the diffuse interstellar medium so they will not escape.** Using a similar technique, Bland-Hawthorn & Maloney (1999) estimated, from the H α emission of the Magellanic stream, that the escape fraction of the Milky Way is $\approx 6\%$. More direct measurements (i.e. based on the observation of the Lyman continuum photons and not on the effect of the ionization), less dependent on geometrical effects, have shown that the escape of Lyman continuum photons from nearby starburst galaxies into the intergalactic medium is probably less than $\approx 10\%$ (e.g. Leitherer et al. 1995, Heckman et al. 2001, Deharveng et al. 2001). This effect is expected to be even less important in normal galaxies than in starbursts, thus it can be discarded as the main responsible for the $f(\text{H}\alpha)/f(\text{UV})$ discrepancy.

3.4. Absorption of Lyman continuum photons by dust

Models of galaxy evolution usually assume that all Lyman continuum photons produce the ionization of one hydrogen atom, contributing to the H α flux. However, if dust is mixed with gas in the star formation regions, only a fraction f' of the Lyman continuum photons will encounter an hydrogen atom, the remaining $(1 - f')$ being absorbed by the dust grains mixed with the ionized gas. This effect, proposed by Inoue et al. (2000) should be properly taken into account to evaluate the energy budget of the star formation regions, thus to calibrate the SFRs of galaxies from Far-IR fluxes. Moreover it also produces a significant shift of the observed $f(\text{H}\alpha)/f(\text{UV})$ ratio with respect to the model predictions. It has been shown by Hirashita et al. (2001) that the absorption of UV photons by dust should not depend much on metallicity, so we can safely assume that this effect will affect in a similar manner all galaxies in our sample. An average value of $f' \approx 0.57$ was found

by Hirashita et al. (2003) for a sample of galaxies similar to ours, assuming approximately constant SFRs over the last $\approx 10^8$ yr. When applying this result to our sample of galaxies we obtain an almost perfect agreement between the observed and expected values of the $f(\text{H}\alpha)/f(\text{UV})$ ratio.

3.5. Non constant SFRs

Galaxies with normal (i.e. “a la Sandage”) SFH, for any τ (fig. 1) can be assumed to have “constant” star formation over the last 10^8 yr. In these conditions the expected $f(\text{H}\alpha)/f(\text{UV})$ is almost constant. However, Table 2 shows that for fixed IMFs or metallicities, non negligible differences of $f(\text{H}\alpha)/f(\text{UV})$ are found for different SFHs. It is then worthwhile to evaluate the consequences of a non-constant SFH on the $f(\text{H}\alpha)/f(\text{UV})$ ratio, which was shown in Table 2 to produce variations on this quantity. A non-constant SFH cannot be discarded if bursts of star formation occurred along the evolution of galaxies. Such events are very likely to have taken place in clusters of galaxies because of galaxy-galaxy and galaxy-IGM interactions.

Fig. 4 shows the effect on the $f(\text{H}\alpha)/f(\text{UV})$ ratio of instantaneous bursts of star formation superposed to the normal evolution assumed “a la Sandage”, with different values of τ . We have represented bursts of intensity 10 and 100 times the expected SFRs for each value of τ . One important point is that the changes in the $f(\text{H}\alpha)/f(\text{UV})$ ratio are insensitive to τ . The plot shows a significant increase of $f(\text{H}\alpha)/f(\text{UV})$ due to the production of stars with $M \geq 8M_{\odot}$ responsible of the H α emission in the first 3×10^6 yr (region **a**), followed by a steep decrease as the burst fades away (region **b**). Some 10^8 yr later, $f(\text{H}\alpha)/f(\text{UV})$ recovers its value previous to the burst (region **c**). The amplitude of both the increase and the decrease of $f(\text{H}\alpha)/f(\text{UV})$ is larger for stronger bursts. We remark that values of $f(\text{H}\alpha)/f(\text{UV})$ significantly lower than the one predicted by models for constant SFR (end of region **b** in the plot) are reached only in the case of bursts of intensities ≥ 10 times the normal current SFRs of galaxies. The presence of the strong burst of star formation can thus account for both a shift and an increase of the dispersion of the $f(\text{H}\alpha)/f(\text{UV})$ distribution.

The temporal dependence of the star formation induced by galaxy interactions is far more complex than just a single instantaneous burst (see Noguchi 1991 and Mihos et al. 1991,1992). The period over which the star formation is enhanced can last for about 10^8 yr. To show the influence of a more complex pattern of star formation on the $f(\text{H}\alpha)/f(\text{UV})$ ratio we show in fig. 5 the $f(\text{H}\alpha)/f(\text{UV})$ evolution for a burst of 10^8 yr duration, overimposed to a normal evolution SFH. In this case, after the first 10^7 yr, the $f(\text{H}\alpha)/f(\text{UV})$ ratio decreases slowly with time and, by 10^8 yr, it converges to the value for normal galaxies.

Once we know the effect of a single star formation burst on the $f(\text{H}\alpha)/f(\text{UV})$ ratio of a single galaxy, we simulate

the expected distributions of $f(\text{H}\alpha)/f(\text{UV})$ for a population of galaxies following a SFH “a la Sandage”, with several overlaid star formation episodes randomly distributed in time. Three parameters are left free in each simulation:

- the time over which all galaxies experience a burst of star formation: 3×10^6 , 10^8 and 10^9 yr, coincident with the timescales of three environmental mechanisms acting on cluster galaxies,
- the duration of the bursts: instantaneous and 10^8 yr,
- the maximum intensity of the burst: 10, 100 and 1000 times the expected SFR for galaxies following an evolution “a la Sandage” at $t = 13$ Gyr.

In order to reproduce a more realistic variety of burst intensities we also produced simulations in which the maximum intensity of the bursts was randomly chosen between 0 and a certain value (namely 10, 100 and 1000 times the normal SFR). By combining the above cases we have reproduced the values of the $f(\text{H}\alpha)/f(\text{UV})$ ratio for 36 scenarios. An error budget consistent with the one of our dataset (detailed in Appendix B) was included in the simulated H α and UV fluxes. For each scenario up to 100 simulations were run. The comparison of the resulting $f(\text{H}\alpha)/f(\text{UV})$ distributions with the observed one are reported in Table 3.

Let us first summarize the scenarios with instantaneous star formation bursts:

- For scenarios 1 to 6, where the star formation episodes are spread along the last 3×10^6 yr, the average $\log f(\text{H}\alpha)/f(\text{UV})$ increases from the theoretical value 1.43, up to 1.91 times. All these scenarios produce distributions of $\log f(\text{H}\alpha)/f(\text{UV})$ non consistent with the observed one, as reflected by the unacceptably high χ_n^2 .
- Scenarios 7 to 12, which correspond to star formation episodes spread along 10^8 yr, show average values of $f(\text{H}\alpha)/f(\text{UV})$ lower than the expected value (strongly depending on the intensity of the star formation episodes). This result is expected since, as shown in fig. 4, after a strong star formation burst the value of $\log f(\text{H}\alpha)/f(\text{UV})$ is below the expected value and it takes about 10^8 yr to recover. It is remarkable that scenarios 9 and 12, which corresponds to star formation bursts of the order of 100 (1000) times the current SFRs, produce $f(\text{H}\alpha)/f(\text{UV})$ distributions consistent with the observed one.
- Finally, scenarios 13 to 18, for which the star formation episodes are spread along 10^9 yr, yield average values of $f(\text{H}\alpha)/f(\text{UV})$ slightly lower than the theoretical one. This means that the effect of an instantaneous burst of star formation is shorter than 10^9 yr. None of these scenarios provide $f(\text{H}\alpha)/f(\text{UV})$ consistent with the observed one.

Concerning the scenarios with bursts of 10^8 yr duration:

- The behavior of scenarios 19 to 30 is similar to that of scenarios 1 to 6, that is, their average $f(\text{H}\alpha)/f(\text{UV})$

ratio is enhanced with respect to the value corresponding to normal galaxies and they show a high average value of χ_n^2 .

- Scenarios 31 to 36 behave like scenarios 7 to 12, with only one of them (namely scenario 33) been fairly consistent with the observed distribution.

Summarizing, we note that bursts of intensities about 100 times the expected SFRs for normal galaxies are required to obtain a $f(\text{H}\alpha)/f(\text{UV})$ distribution consistent with the one observed in our sample galaxies, under the assumption that non constant star formation is the only mechanism governing the $f(\text{H}\alpha)/f(\text{UV})$ ratio.

4. Discussion

In the previous section we explored some physical mechanisms that could possibly explain the inconsistency between the observed distribution of $f(\text{H}\alpha)/f(\text{UV})$ and the theoretical value. We reached the conclusion that, while the dispersion is consistent with the observational uncertainties, the difference between the average observed value of $f(\text{H}\alpha)/f(\text{UV})$ and the theoretical value is real and might have physical implications. Of all the explored possibilities only two seem able to reproduce the observed $f(\text{H}\alpha)/f(\text{UV})$ distribution, namely: non constant SFRs over the last 10^8 yr and the absorption of Lyman continuum photons by dust within star forming regions.

The non constant SFR hypothesis has been used by Sullivan et al. (2000, 2001) to explain the discrepancy between the observed and the theoretical H α and UV fluxes in a sample of UV selected galaxies. For galaxies in clusters, where interactions are likely to take place, the “non constant” star formation scenario seems the realistic one. However, since not all cluster galaxies are affected by the environment in the same way, we split our sample in several subsamples in order to study the behavior of the $f(\text{H}\alpha)/f(\text{UV})$ distributions for galaxies in various evolutionary stages:

- Galaxies showing clear morphological disturbances are known to be experiencing recent interactions with close neighbors or with the IGM, and in most cases an enhancement of their SFRs is reflected on their H α fluxes (timescale for production of Lyman continuum photons $\leq 10^7$ yr). Three galaxies of our sample belong to this category: CGCG 097-073 and CGCG 097-079 (Gavazzi et al. 2001a) and CGCG 097-087 (Gavazzi et al. 2001b). These galaxies will be referred hereafter as the “*interacting*” subsample.
- Galaxies with asymmetric HI profiles are known to have experienced interactions on timescales of $\simeq 5 \times 10^8$ yr (Gavazzi 1989), corresponding to the timescale necessary for redistributing the neutral gas throughout the disk. In our sample, these are the galaxies labeled “A” in last column of Table 1. Hereafter, we will re-

fer to them as the “*asymmetric*” subsample¹. Given that the timescale for removing the HI asymmetries is usually larger than the timescale over which the effects of the interactions are apparent (i.e. close galaxy-galaxy interactions), the enhancement of the SFRs for these galaxies is expected to be lower than for the “*interacting*” ones.

- Another measure of the interaction with the environment is provided by the HI deficiency parameter. As galaxies approach the cluster center they lose their peripheral gas envelope due to ram-pressure stripping, preventing their subsequent star formation. The timescale for this process is $\simeq 10^9$ yr, which approximately corresponds to the cluster crossing time. We consider as “*deficient*” galaxies those with $def(HI) \geq 0.4$. We exclude from this subsample deficient galaxies with asymmetric profiles, in order to separate the effects of HI deficiency from interactions.
- Finally, we define a “*reference*” sample of galaxies for which no traces of interaction with the cluster environment are found: they have a normal HI content (i.e., $def(HI) < 0.4$) and do not show neither clear signatures of interactions nor asymmetric HI profiles. These galaxies will be considered hereafter as “normal” galaxies.

Table 4 lists the average values of the $f(H\alpha)/f(UV)$ and b_{obs}/b_{model} ratios for each different subsample. Figs. 7 and 8 show the $f(H\alpha)/f(UV)$ and b_{obs}/b_{model} ratios of the individual galaxies of the three subsamples vs. their HI deficiency.

The “*reference*” galaxies show $\langle \log b_{obs}/b_{model} \rangle = 0$, meaning that their recent star formation activity coincides with the expected one. In addition, $\langle \log f(H\alpha)/f(UV) \rangle = 1.11$, which does not correspond to the theoretical value of 1.43 predicted by synthesis models. Given that these galaxies are selected for their normal HI content and no traces of interactions, we take this value as a reference value for normal star forming galaxies. Absorption of $\simeq 45\%$ Lyman continuum photons by dust within HII regions should account for the discrepancy between the observed and theoretical value of the $f(H\alpha)/f(UV)$ ratio for normal galaxies.

Moving on to galaxies perturbed by the cluster environment, we find that the “*interacting*” and “*asymmetric*” galaxies show values of $\log f(H\alpha)/f(UV)$ 0.14 dex higher than “*reference*” galaxies. As we showed in Section 3.5, the presence of star formation bursts is likely to produce such an enhancement. From the b_{obs}/b_{model} ratio we estimate that the intensity of the star formation activity is at present 3.5 times higher for the “*interacting*” galaxies compared to the *asymmetric* and the “*reference*” ones. Given that the “*interacting*” galaxies are presently undergoing an interaction, the age of the burst is $\approx 10^6$ yr, thus the increase of the star formation activity is maximal

¹ In order to avoid confusion, we do not include the galaxies from the “*interacting*” subsample in the “*asymmetric*” subsample, although these three galaxies show an asymmetric profile.

(see fig. 4). We thus expect that, consistently with model predictions (Fujita 1998), galaxy-galaxy or galaxy-IGM interactions in clusters can induce bursts of star formation able to increase by up to a factor of ≈ 4 the expected SFR of normal late-type galaxies.

Finally, we analyze the behavior of the “*deficient*” galaxies. These galaxies have been shown to have lower than expected star formation activity as measured by the b parameter (Boselli et al. 2001). However, we find for them higher $f(H\alpha)/f(UV)$ and of b_{obs}/b_{model} than for the “*reference*” galaxies. This apparent contradiction might be due to selection effects. To illustrate this point we show in Table 5 the average values of $EW(H\alpha + [NII])$ for subsamples of galaxies satisfying the various observational constraints, separately for deficient and non deficient galaxies. It appears that, as more observational constraints are applied, the resulting average $EW(H\alpha + [NII])$ tends to increase, biasing towards more actively star forming galaxies. For the non deficient galaxies, this bias affects the average $EW(H\alpha + [NII])$ by less than 30%. For the deficient galaxies, by imposing the condition for H β line detection, the estimate of $EW(H\alpha + [NII])$ results doubled. The “*reference*”, “*interacting*” and “*asymmetric*” samples are less affected by this selection bias because they contain non-deficient objects.

5. Conclusions

The $f(H\alpha)/f(UV)$ ratio of cluster galaxies is analyzed in this paper as a promising tool to estimate if the star formation history of galaxies has remained constant on timescales of $\simeq 10^8$ yr. The observed $f(H\alpha)/f(UV)$ distribution is compared to the one predicted by models of galaxies, assuming a continuum SFH. The dispersion of the observed $f(H\alpha)/f(UV)$ distribution is consistent with the one expected from the observational uncertainties. We find a systematic negative difference between the average observed value and the model predictions. We discuss some mechanisms that could possibly produce such an observed difference and we highlight the two most likely ones: the absorption and, in a minor way, the escape of Lyman continuum photons and the occurrence of star formation bursts overimposed to a smooth SFH.

The $f(H\alpha)/f(UV)$ distribution is considered for different galaxy subsamples, each of them comprising galaxies in different evolutionary stages, possibly induced by the cluster environment. The “*reference*” unperturbed galaxies have $f(H\alpha)/f(UV)$ lower by 0.34 dex on average than the one predicted by the models. We suggest that absorption (and to a lesser extent escape) of Lyman continuum photons causes the observed discrepancy. We estimate that about 45% of the Lyman continuum photons are absorbed by dust in the star forming regions before ionization, consistently with the estimate of Hirashita et al. (2003) on similar objects.

When galaxies with signatures of recent or past interactions with the cluster environment (“*interacting*” and “*asymmetric*”) are considered, we find that their

$f(\text{H}\alpha)/f(\text{UV})$ ratio is slightly higher than the one of “reference” galaxies. Even though the absorption of Lyman continuum photons is taken into account, the observed $f(\text{H}\alpha)/f(\text{UV})$ ratio can be reconciled to the predicted one only assuming that these objects underwent bursts of star formation of intensity ~ 100 times larger than normal, as intense as Arp 220. Objects of this kind are however not presently observed in nearby clusters.

The present observational uncertainties on both the H α and UV fluxes are still too large to allow disentangling the effects of recent star formation bursts from those of absorption of Lyman continuum photons. However we stress the potentiality of the proposed H α /UV method for studying the recent history of star formation in late type galaxies, once improvements in modeling the radiation transfer through the dust in star forming regions will be achieved and more precise UV and Far-IR photometry will be available. This will soon become a reality after the GALEX and ASTRO-F experiments will perform their all sky surveys, providing $\Delta f(\text{UV})$ and $\Delta f(\text{Far-IR}) \approx 10\%$.

Acknowledgements. We thank Veronique Buat and Jean Michel Deharveng for interesting comments and suggestions. JIP acknowledges the Fifth Framework Program of the EU for a Marie Curie Postdoctoral Fellowship. This research has made use of the NASA/IPAC Extragalactic Database (NED) and of the NASA/ IPAC Infrared Science Archive, which are operated by the Jet Propulsion Laboratory, California Institute of Technology, under contract with the National Aeronautics and Space Administration. We also acknowledge the GOLD Mine Database, operated by the Università degli Studi di Milano-Bicocca.

References

- Abadi, M. G., Moore, B., & Bower, R. G. 1999, M.N.R.A.S., 308, 947
- Balogh, M. L., Morris, S. L., Yee, H. K. C., Carlberg, R. G., & Ellingson, E. 1999, Ap.J., 527, 54
- Barger, A. J., Aragon-Salamanca, A., Ellis, R. S., Couch, W. J., Smail, I., & Sharples, R. M. 1996, M.N.R.A.S., 279, 1
- Bergvall, N., Laurikainen, E., & Aalto, S. 2003, A. & A., 405, 31
- Binggeli, B., Sandage, A., & Tammann, G. A. 1985, A.J., 90, 1681
- Binggeli, B. & Cameron, L. M. 1993, A. & A.S., 98, 297
- Bland-Hawthorn, J. & Maloney, P. R. 1999, Ap.J., 510, L33
- Boselli, A., Gavazzi, G., Donas, J., & Scodreggio, M. 2001, A.J., 121, 753
- Boselli, A. & Gavazzi, G. 2002, A. & A., 386, 124
- Boselli, A., Iglesias-Páramo, J., Vílchez, J. M., & Gavazzi, G. 2002, A. & A., 386, 134
- Boselli, A., Gavazzi, G., & Sanvito, G. 2003, A. & A., 402, 37
- Bothun, G. D., Aaronson, M., Schommer, B., Mould, J., Huchra, J., & Sullivan, W. T. 1985, Ap.J.S., 57, 423
- Bravo-Alfaro, H., Cayatte, V., van Gorkom, J. H., & Balkowski, C. 2001, A. & A., 379, 347
- Buat, V., Donas, J., & Deharveng, J. M. 1987, A. & A., 185, 33
- Buat, V. & Xu, C. 1996, A. & A., 306, 61
- Buat, V., Donas, J., Milliard, B., & Xu, C. 1999, A. & A., 352, 371
- Buat, V., Boselli, A., Gavazzi, G., & Bonfanti, C. 2002, A. & A., 383, 801
- Burstein, D. & Heiles, C. 1982, A.J., 87, 1165
- Butcher, H. & Oemler, A. 1978, Ap.J., 226, 559
- Byrd, G. & Valtonen, M. 1990, Ap.J., 350, 89
- Charlot, S. & Longhetti, M. 2001, M.N.R.A.S., 323, 887
- Chincarini, G. L., Giovanelli, R., Haynes, M., & Fontanelli, P. 1983, Ap.J., 267, 511
- Couch, W. J. & Sharples, R. M. 1987, M.N.R.A.S., 229, 423
- Couch, W. J., Ellis, R. S., Sharples, R. M., & Smail, I. 1994, Ap.J., 430, 121
- Deharveng, J.-M., Sasseen, T. P., Buat, V., Bowyer, S., Lampton, M., & Wu, X. 1994, A. & A., 289, 715
- Deharveng, J.-M., Buat, V., Le Brun, V., Milliard, B., Kunth, D., Shull, J. M., & Gry, C. 2001, A. & A., 375, 805
- Eisenhauer, F., Quirrenbach, A., Zinnecker, H., & Genzel, R. 1998, Ap.J., 498, 278
- Figer, D. F., Kim, S. S., Morris, M., Serabyn, E., Rich, R. M., & McLean, I. S. 1999, Ap.J., 525, 750
- Fujita, Y. 1998, Ap.J., 509, 587
- Fujita, Y. & Nagashima, M. 1999, Ap.J., 516, 619
- Gavazzi, G. 1987, Ap.J., 320, 96
- Gavazzi, G. 1989, Ap.J., 346, 59
- Gavazzi, G., Boselli, A., & Kennicutt, R. 1991, A.J., 101, 1207
- Gavazzi, G. & Boselli, A. 1996, Astrophysical Letters Communications, 35, 1
- Gavazzi, G., Catinella, B., Carrasco, L., Boselli, A., & Contursi, A. 1998, A.J., 115, 1745
- Gavazzi, G., Boselli, A., Scodreggio, M., Pierini, D., & Belsole, E. 1999, M.N.R.A.S., 304, 595
- Gavazzi, G., Boselli, A., Mayer, L., Iglesias-Paramo, J., Vílchez, J. M., & Carrasco, L. 2001a, Ap.J., 563, L23
- Gavazzi, G., Marcelin, M., Boselli, A., Amram, P., Vílchez, J. M., Iglesias-Paramo, J., & Tarenghi, M. 2001b, A. & A., 377, 745
- Gavazzi, G., Bonfanti, C., Sanvito, G., Boselli, A., & Scodreggio, M. 2002a, Ap.J., 576, 135
- Gavazzi, G., Boselli, A., Pedotti, P., Gallazzi, A., & Carrasco, L. 2002b, A. & A., 386, 114
- Gavazzi, G., Boselli, A., Donati, A., Franzetti, P., & Scodreggio, M. 2003, A. & A., 400, 451
- Giovanelli, R. & Haynes, M. P. 1985, Ap.J., 292, 404
- Gunn, J. E. & Gott, J. R. I. 1972, Ap.J., 176, 1
- Haynes, M. P. & Giovanelli, R. 1984, A.J., 89, 758
- Haynes, M. P. & Giovanelli, R. 1986, Ap.J., 306, 466
- Heckman, T. M., Sembach, K. R., Meurer, G. R., Leitherer, C., Calzetti, D., & Martin, C. L. 2001, Ap.J., 558, 56
- Helou, G., Hoffman, G. L., & Salpeter, E. E. 1984, Ap.J.S., 55, 433
- Hirashita, H., Inoue, A. K., Kamaya, H., & Shibai, H. 2001, A. & A., 366, 83
- Hirashita, H., Buat, V., & Inoue, A. K. 2003, A. & A., 410, 83
- Hoffman, G. L., Williams, H. L., Salpeter, E. E., Sandage, A., & Binggeli, B. 1989, Ap.J.S., 71, 701
- Hummel, E., van der Hulst, J. M., Keel, W. C., & Kennicutt, R. C. 1987, A. & A.S., 70, 517
- Iglesias-Páramo, J., Boselli, A., Cortese, L., Vílchez, J. M., & Gavazzi, G. 2002, A. & A., 384, 383
- Inoue, A. K., Hirashita, H., & Kamaya, H. 2000, P.A.S.J., 52, 539
- Kennicutt, R. C. & Kent, S. M. 1983, A.J., 88, 1094
- Kennicutt, R. C., Bothun, G. D., & Schommer, R. A. 1984, A.J., 89, 1279

- Kennicutt, R. C., Roettiger, K. A., Keel, W. C., van der Hulst, J. M., & Hummel, E. 1987, *A.J.*, 93, 1011
- Kennicutt, R. C. 1992, *Ap.J.*, 388, 310
- Kennicutt, R. C., Tamblyn, P., & Congdon, C. E. 1994, *Ap.J.*, 435, 22
- Kennicutt, R. C. 1998, *A.R.A. & A.*, 36, 189
- Lampton, M., Deharveng, J. M., & Bowyer, S. 1990, *IAU Symp. 139: The Galactic and Extragalactic Background Radiation*, 139, 449
- Larson, R. B. & Tinsley, B. M. 1978, *Ap.J.*, 219, 46
- Leitherer, C., Ferguson, H. C., Heckman, T. M., & Lowenthal, J. D. 1995, *Ap.J.*, 454, L19
- Leitherer, C. et al. 1999, *Ap.J.S.*, 123, 3
- Lequeux, J., Maucherat-Joubert, M., Deharveng, J. M., & Kunth, D. 1981, *A. & A.*, 103, 305
- Madau, P., Pozzetti, L., & Dickinson, M. 1998, *Ap.J.*, 498, 106
- Massey, P. 1998, *Ap.J.*, 501, 153
- Massey, P. & Hunter, D. A. 1998, *Ap.J.*, 493, 180
- Mihos, J. C., Richstone, D. O., & Bothun, G. D. 1991, *Ap.J.*, 377, 72
- Mihos, J. C., Richstone, D. O., & Bothun, G. D. 1992, *Ap.J.*, 400, 153
- Miller, G. E. & Scalo, J. M. 1979, *Ap.J.S.*, 41, 513
- Milliard, B., Donas, J., & Laget, M. 1991, *Advances in Space Research*, 11, 135
- Moore, B., Katz, N., Lake, G., Dressler, A., & Oemler, A. 1996, *Nature*, 379, 613
- Moshir, M. 1989, *Pasadena: Infrared Processing and Analysis Center, California Institute of Technology, 1989*, edited by Moshir, M.,
- Noguchi, M. 1991, *M.N.R.A.S.*, 251, 360
- Osterbrock, D. E. 1989, *Research supported by the University of California, John Simon Guggenheim Memorial Foundation, University of Minnesota, et al. Mill Valley, CA, University Science Books, 1989*, 422 p.
- Poggianti, B. M., Smail, I., Dressler, A., Couch, W. J., Barger, A. J., Butcher, H., Ellis, R. S., & Oemler, A. J. 1999, *Ap.J.*, 518, 576
- Rosa-González, D., Terlevich, E., & Terlevich, R. 2002, *M.N.R.A.S.*, 332, 283
- Sakhibov, F. & Smirnov, M. 2000, *A. & A.*, 354, 802
- Schneider, S. E., Thuan, T. X., Magri, C., & Wadiak, J. E. 1990, *Ap.J.S.*, 72, 245
- Soifer, B. T. et al. 1984, *Ap.J.*, 278, L71
- Sullivan, M., Treyer, M. A., Ellis, R. S., Bridges, T. J., Milliard, B., & Donas, J. 2000, *M.N.R.A.S.*, 312, 442
- Sullivan, M., Mobasher, B., Chan, B., Cram, L., Ellis, R., Treyer, M., & Hopkins, A. 2001, *Ap.J.*, 558, 72
- Zurita, A., Rozas, M., & Beckman, J. E. 2000, *A. & A.*, 363, 9
- Zwicky, F., Herzog, E., & Wild, P. 1968, *Pasadena: California Institute of Technology (CIT), 1961-1968*,

Table 1. Basic properties and observational data of the sample galaxies.

Name	$\log f(\text{H}\alpha)$ ($\text{erg s}^{-1} \text{cm}^{-2}$)	$\log f(\text{UV})$ ($\text{erg s}^{-1} \text{cm}^{-2} \text{\AA}^{-1}$)	$\log L_{\text{H}}$ (L_{\odot})	$def(\text{H}\text{I})$	H I asymm.
VCC 25	-11.59	-12.75	10.39	-0.21	?
VCC 66	-11.48	-12.89	10.22	-0.20	?
VCC 89	-11.74	-12.78	10.65	-0.03	S
VCC 92	-11.21	-12.33	10.99	0.33	?
VCC 131	-12.60	-13.30	9.52	0.09	S
VCC 157	-11.31	-12.65	10.48	0.61	S
VCC 221	-11.94	-13.12	9.88	0.41	S
VCC 307	-10.73	-11.95	10.94	0.01	S
VCC 318	-12.48	-13.68	9.18	-0.13	S
VCC 382	-12.05	-12.59	10.65	-0.32	S
VCC 459	-12.58	-13.61	8.73	-0.07	S
VCC 491	-11.75	-12.89	9.42	-0.29	S
VCC 508	-10.72	-11.86	10.98	-0.06	S
VCC 552	-12.23	-13.29	8.99	-0.42	S
VCC 664	-12.17	-13.38	8.92	0.62	S
VCC 667	-12.75	-13.71	9.78	0.58	S
VCC 692	-12.50	-13.36	9.64	0.66	S
VCC 699	-12.37	-13.31	9.71	0.19	S
VCC 787	-12.47	-13.35	9.65	0.26	S
VCC 801	-11.58	-13.12	9.97	-0.62	S
VCC 827	-12.10	-13.15	10.14	0.08	S
VCC 836	-11.51	-12.57	10.54	0.69	S
VCC 849	-12.11	-13.36	9.79	0.41	S
VCC 851	-12.18	-13.79	9.80	0.23	A
VCC 865	-11.86	-13.12	9.69	0.38	S
VCC 873	-11.15	-12.79	10.39	0.63	S
VCC 905	-12.63	-13.59	9.66	0.35	S
VCC 912	-12.19	-13.26	9.88	0.99	S
VCC 921	-11.89	-13.05	9.64	0.59	S
VCC 938	-12.09	-13.26	9.74	0.36	S
VCC 939	-12.32	-13.18	9.87	0.24	S
VCC 957	-11.64	-12.90	9.91	0.02	?
VCC 971	-12.40	-13.55	9.50	0.20	?
VCC 979	-11.98	-13.14	10.45	1.17	S
VCC 980	-12.52	-13.55	8.77	0.67	?
VCC 1002	-11.65	-13.21	10.22	0.47	S
VCC 1091	-12.22	-13.47	8.86	-0.35	S
VCC 1118	-12.08	-13.27	10.08	0.51	S
VCC 1189	-12.55	-13.65	9.25	0.34	A
VCC 1193	-12.43	-13.79	9.28	-0.05	S
VCC 1205	-12.41	-13.02	9.73	-0.03	S
VCC 1290	-12.20	-13.18	9.91	0.05	S
VCC 1379	-12.09	-13.07	9.84	0.15	S
VCC 1393	-12.22	-13.32	9.47	0.23	S
VCC 1401	-10.76	-12.20	11.18	0.55	S
VCC 1450	-12.01	-12.99	9.47	0.54	S
VCC 1508	-11.59	-12.75	9.93	-0.26	S
VCC 1516	-11.77	-13.19	9.85	0.80	S
VCC 1532	-12.35	-13.44	9.55	0.82	S
VCC 1554	-11.28	-12.56	9.90	-0.37	S

Table 1. Continued.

Name	$\log f(\text{H}\alpha)$ ($\text{erg s}^{-1} \text{cm}^{-2}$)	$\log f(\text{UV})$ ($\text{erg s}^{-1} \text{cm}^{-2} \text{\AA}^{-1}$)	$\log L_{\text{H}}$ (L_{\odot})	$def(\text{H}\text{I})$	H I asymm.
VCC 1575	-11.08	-12.27	10.76	0.19	S
VCC 1588	-12.04	-13.05	10.05	0.68	S
VCC 1678	-12.45	-13.62	8.81	-0.06	S
VCC 1699	-12.90	-13.75	8.83	0.04	S
VCC 1725	-12.70	-13.74	8.97	0.55	S
VCC 1811	-12.31	-13.21	9.85	0.23	S
VCC 1929	-12.63	-13.34	9.51	0.35	S
VCC 1943	-11.43	-12.95	10.26	0.25	S
VCC 1972	-11.32	-12.66	10.50	0.27	S
VCC 1987	-11.23	-12.31	10.66	-0.29	A
VCC 2058	-11.15	-12.91	10.35	0.90	S
CGCG 043-034	-11.42	-12.86	9.79	-0.29	S
CGCG 043-071	-11.32	-12.68	10.12	-0.75	S
CGCG 043-093	-11.43	-12.64	10.27	-0.07	S
CGCG 097-062	-12.97	-14.30	10.10	0.31	A
CGCG 097-068	-11.74	-13.43	10.78	-0.14	S
CGCG 097-073	-12.77	-14.07	10.00	0.16	A
CGCG 097-079	-12.70	-13.87	10.02	0.25	A
CGCG 097-087	-11.97	-13.25	10.88	0.19	A
CGCG 097-091	-12.69	-13.67	10.85	-0.18	S
CGCG 097-120	-12.13	-13.75	11.06	0.90	S
CGCG 100-004	-11.33	-12.60	10.52	-0.24	S
CGCG 119-029	-12.13	-13.34	10.75	-0.30	S
CGCG 119-041	-12.83	-13.74	10.51	0.30	S
CGCG 119-043	-12.70	-13.94	10.07	0.29	S
CGCG 119-046	-12.15	-13.39	10.32	-0.22	S
CGCG 119-047	-12.42	-13.43	10.42	-0.61	S
CGCG 119-053	-13.00	-13.98	10.12	-0.37	S
CGCG 119-054	-12.44	-13.91	10.70	—	?
CGCG 119-059	-13.13	-13.93	9.66	0.14	S
CGCG 119-068	-12.66	-13.84	10.40	-0.27	S
CGCG 119-085	-13.61	-14.19	10.38	-0.17	S
CGCG 127-049	-12.52	-13.88	10.51	0.32	S
CGCG 160-020	-13.00	-13.82	9.98	0.27	S
CGCG 160-026	-12.96	-14.11	10.31	0.23	A
CGCG 160-055	-12.56	-13.41	10.96	0.49	A
CGCG 160-058	-12.65	-14.00	10.58	0.40	S
CGCG 160-067	-12.62	-13.86	10.06	-0.05	S
CGCG 160-076	-12.88	-14.08	9.87	-0.35	S
CGCG 160-086	-12.84	-14.09	10.05	0.76	?
CGCG 160-088	-12.06	-14.04	10.88	0.42	S
CGCG 160-106	-12.55	-13.90	10.99	0.54	?
CGCG 160-108	-12.92	-14.09	10.16	—	?
CGCG 160-128	-12.73	-13.91	9.86	—	?
CGCG 160-139	-12.60	-13.81	10.02	-0.19	A
CGCG 160-213	-12.72	-13.81	10.10	—	?
CGCG 160-252	-12.49	-13.55	10.38	0.56	S
CGCG 160-260	-12.47	-13.64	11.21	0.81	S

Table 2. Dependence of the $f(\text{H}\alpha)/f(\text{UV})$ ratio on the IMF parameters, metallicity and star formation history: (1) Evolutionary synthesis code; (2) Metallicity; (3) IMF slope; (4) Lower limit for the IMF; (5) Upper limit for the IMF; (6) Time interval over which the SFR is considered constant; (7) log of the $f(\text{H}\alpha)/f(\text{UV})$ ratio.

Source	Z	IMF	M_{low}	M_{up}	t	$\log f(\text{H}\alpha)/f(\text{UV})$
PEGASE2	0.0004	Salpeter	1	100	10^7	1.79
PEGASE2	0.004	Salpeter	1	100	10^7	1.69
PEGASE2	0.02	Salpeter	1	100	10^7	1.51
PEGASE2	0.05	Salpeter	1	100	10^7	1.35
Starburst99	0.001	Salpeter	1	100	10^7	1.75
Starburst99	0.004	Salpeter	1	100	10^7	1.67
Starburst99	0.008	Salpeter	1	100	10^7	1.63
Starburst99	0.020	Salpeter	1	100	10^7	1.57
Starburst99	0.040	Salpeter	1	100	10^7	1.51
PEGASE2	0.0004	Salpeter	1	100	10^8	1.54
PEGASE2	0.004	Salpeter	1	100	10^8	1.46
PEGASE2	0.02	Salpeter	1	100	10^8	1.33
PEGASE2	0.05	Salpeter	1	100	10^8	1.20
Starburst99	0.001	Salpeter	1	100	10^8	1.50
Starburst99	0.004	Salpeter	1	100	10^8	1.44
Starburst99	0.008	Salpeter	1	100	10^8	1.42
Starburst99	0.020	Salpeter	1	100	10^8	1.38
Starburst99	0.040	Salpeter	1	100	10^8	1.34
Starburst99	0.001	Salpeter	1	30	10^8	1.04
Starburst99	0.004	Salpeter	1	30	10^8	0.93
Starburst99	0.008	Salpeter	1	30	10^8	0.88
Starburst99	0.020	Salpeter	1	30	10^8	0.80
Starburst99	0.040	Salpeter	1	30	10^8	0.78
Starburst99	0.001	Miller-Scalo	1	100	10^8	0.95
Starburst99	0.004	Miller-Scalo	1	100	10^8	0.89
Starburst99	0.008	Miller-Scalo	1	100	10^8	0.86
Starburst99	0.020	Miller-Scalo	1	100	10^8	0.82
Starburst99	0.040	Miller-Scalo	1	100	10^8	0.78

Table 3. The simulated scenarios for instantaneous bursts of star formation: (1) Identifier of the model; (2) Time interval over which all simulated galaxies experience a burst of star formation (yr); (3) Duration of the burst (yr); (4) Maximum intensity of the burst in units of the expected SFR of galaxies following an evolution “a la Sandage” at $t = 13$ Gyr; (5) Average χ_n^2 between the observed and each of the simulated distributions; (6) Average value of $f(\text{H}\alpha)/f(\text{UV})$ for 100 simulated distributions; (7) Average of $\sigma f(\text{H}\alpha)/f(\text{UV})$ for 100 simulated distributions.

Id.	Δt	Duration	Intensity	$\langle \chi_n^2 \rangle$	$\langle \log f(\text{H}\alpha)/f(\text{UV}) \rangle$	$\langle \sigma \rangle$
1	3×10^6	Inst.	10 for all galaxies	7.39 ± 0.98	1.71	0.22
2	3×10^6	Inst.	Random between 0 and 10	6.20 ± 0.98	1.58	0.26
3	3×10^6	Inst.	100 for all galaxies	6.17 ± 1.44	1.90	0.23
4	3×10^6	Inst.	Random between 0 and 100	6.94 ± 1.13	1.81	0.24
5	3×10^6	Inst.	1000 for all galaxies	6.04 ± 1.47	1.91	0.23
6	3×10^6	Inst.	Random between 0 and 1000	5.88 ± 1.25	1.91	0.26
7	10^8	Inst.	10 for all galaxies	2.62 ± 0.70	1.41	0.26
8	10^8	Inst.	Random between 0 and 10	2.71 ± 0.61	1.39	0.25
9	10^8	Inst.	100 for all galaxies	0.87 ± 0.38	1.25	0.28
10	10^8	Inst.	Random between 0 and 100	1.53 ± 0.48	1.37	0.26
11	10^8	Inst.	1000 for all galaxies	3.03 ± 0.74	0.92	0.42
12	10^8	Inst.	Random between 0 and 1000	1.03 ± 0.38	1.12	0.39
13	10^9	Inst.	10 for all galaxies	2.67 ± 0.62	1.35	0.23
14	10^9	Inst.	Random between 0 and 10	2.84 ± 0.66	1.41	0.22
15	10^9	Inst.	100 for all galaxies	2.46 ± 0.66	1.35	0.23
16	10^9	Inst.	Random between 0 and 100	2.68 ± 0.74	1.34	0.23
17	10^9	Inst.	1000 for all galaxies	1.59 ± 0.53	1.31	0.34
18	10^9	Inst.	Random between 0 and 1000	1.84 ± 0.45	1.39	0.27
19	3×10^6	10^8	10 for all galaxies	7.53 ± 0.96	1.73	0.26
20	3×10^6	10^8	Random between 0 and 10	4.88 ± 0.78	1.53	0.27
21	3×10^6	10^8	100 for all galaxies	6.35 ± 1.17	1.88	0.25
22	3×10^6	10^8	Random between 0 and 100	6.87 ± 1.23	1.82	0.24
23	3×10^6	10^8	1000 for all galaxies	6.05 ± 1.31	1.91	0.24
24	3×10^6	10^8	Random between 0 and 1000	6.04 ± 1.42	1.92	0.24
25	10^8	10^8	10 for all galaxies	5.48 ± 0.83	1.53	0.24
26	10^8	10^8	Random between 0 and 10	4.98 ± 0.78	1.50	0.23
27	10^8	10^8	100 for all galaxies	5.84 ± 0.79	1.55	0.22
28	10^8	10^8	Random between 0 and 100	5.68 ± 0.82	1.53	0.23
29	10^8	10^8	1000 for all galaxies	5.62 ± 0.82	1.59	0.27
30	10^8	10^8	Random between 0 and 1000	5.58 ± 0.88	1.57	0.26
31	10^9	10^8	10 for all galaxies	1.87 ± 0.51	1.37	0.26
32	10^9	10^8	Random between 0 and 10	2.33 ± 0.58	1.38	0.25
33	10^9	10^8	100 for all galaxies	1.11 ± 0.40	1.09	0.47
34	10^9	10^8	Random between 0 and 100	1.28 ± 0.42	1.19	0.37
35	10^9	10^8	1000 for all galaxies	1.94 ± 0.50	0.68	0.70
36	10^9	10^8	Random between 0 and 1000	1.31 ± 0.40	0.88	0.66

Table 4. Averaged values of $f(\text{H}\alpha)/f(\text{UV})$ and $\log b_{\text{obs}}/b_{\text{model}}$ for the various analyzed subsamples. Numbers in parenthesis correspond to one standard deviation.

Subsample	Num. gal.	$\langle def(\text{HI}) \rangle$	$\langle \log f(\text{H}\alpha)/f(\text{UV}) \rangle$	$\langle \log b_{\text{obs}}/b_{\text{model}} \rangle$
<i>Reference</i>	57	-0.03(0.28)	1.11(0.24)	0.00(0.41)
<i>Interacting</i>	3	0.20(0.05)	1.25(0.07)	0.55(0.41)
<i>Asymmetric</i>	6	0.11(0.27)	1.24(0.20)	0.01(0.34)
<i>Deficient</i>	27	0.66(0.18)	1.25(0.27)	0.07(0.50)

Table 5. Average star formation activity in subsamples satisfying various selection criteria.

Observational constraint	$\langle EW(\text{H}\alpha + [\text{NII}]) \rangle$ (\AA)		
	All	$def(\text{H}\alpha) < 0.4$	$def(\text{H}\alpha) \geq 0.4$
None	17	22	10
FIR det.	19	24	11
UV det.	21	28	12
FIR & UV det.	23	31	13
H β det.	27	29	20

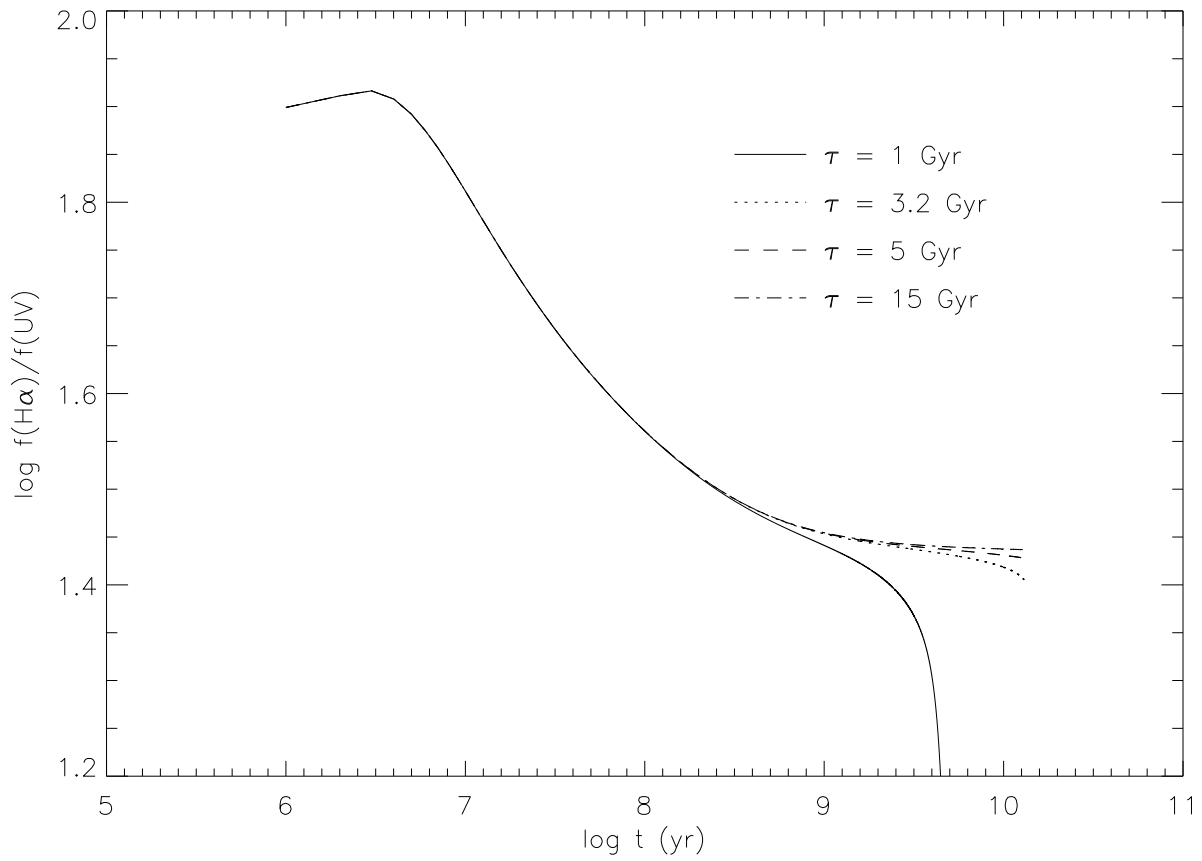


Fig. 1. Evolution of the $f(\text{H}\alpha)/f(\text{UV})$ ratio with time for galaxies with SFH “a la Sandage”, for values of $\tau = 1, 3.2, 5$ and 15 Gyr. The Salpeter IMF and solar metallicity are assumed.

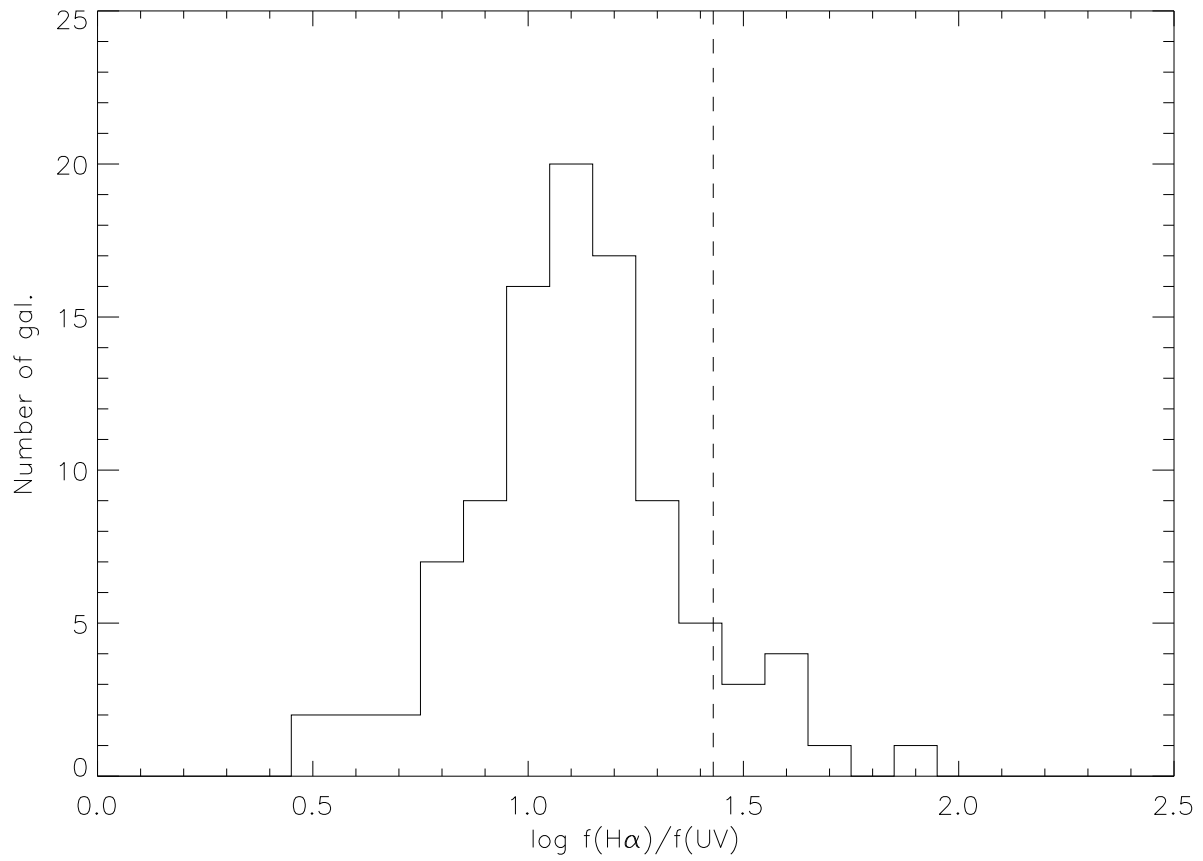


Fig. 2. Histogram of the observed $f(H\alpha)/f(UV)$ ratio for galaxies in our sample. The dashed line corresponds to the average expected value for evolutionary models “à la Sandage”.

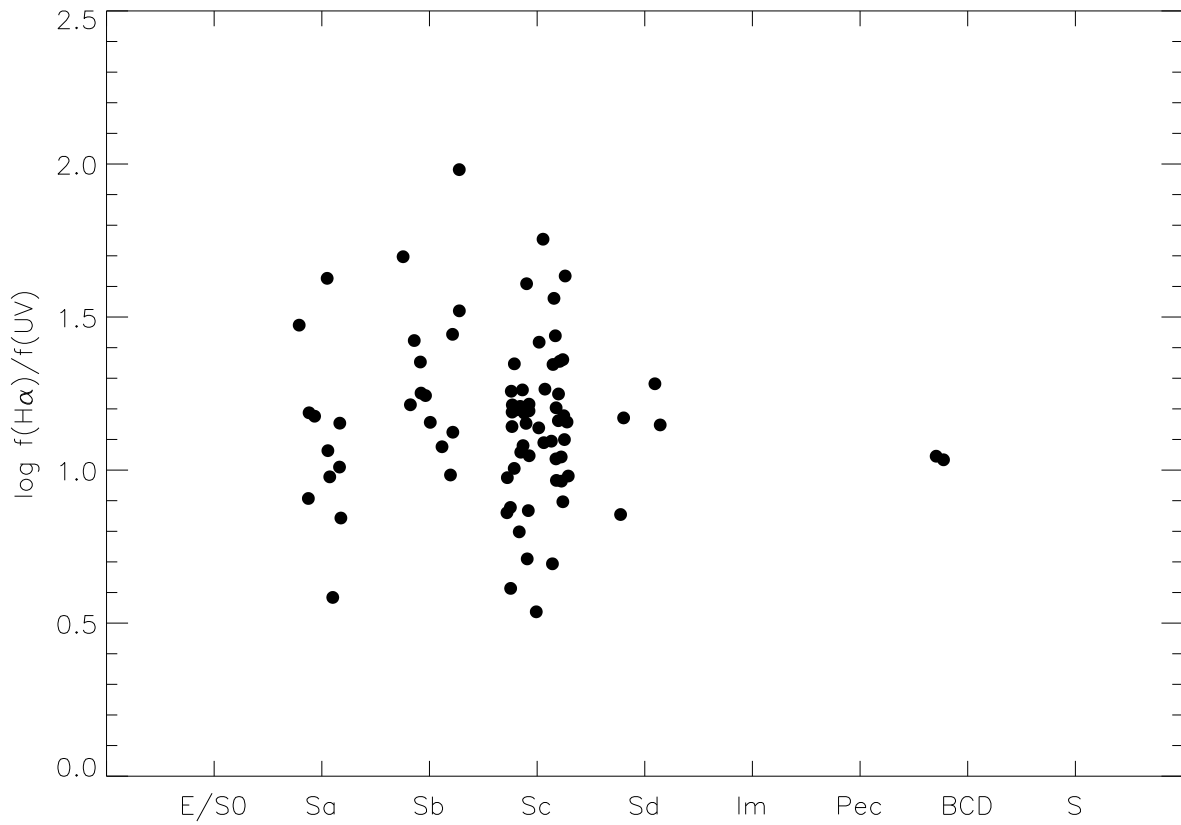


Fig. 3. $f(H\alpha)/f(UV)$ ratio vs. the Hubble type for all galaxies in our sample. A random value between -0.4 and 0.4 has been added to each numerical type to avoid overplotting.

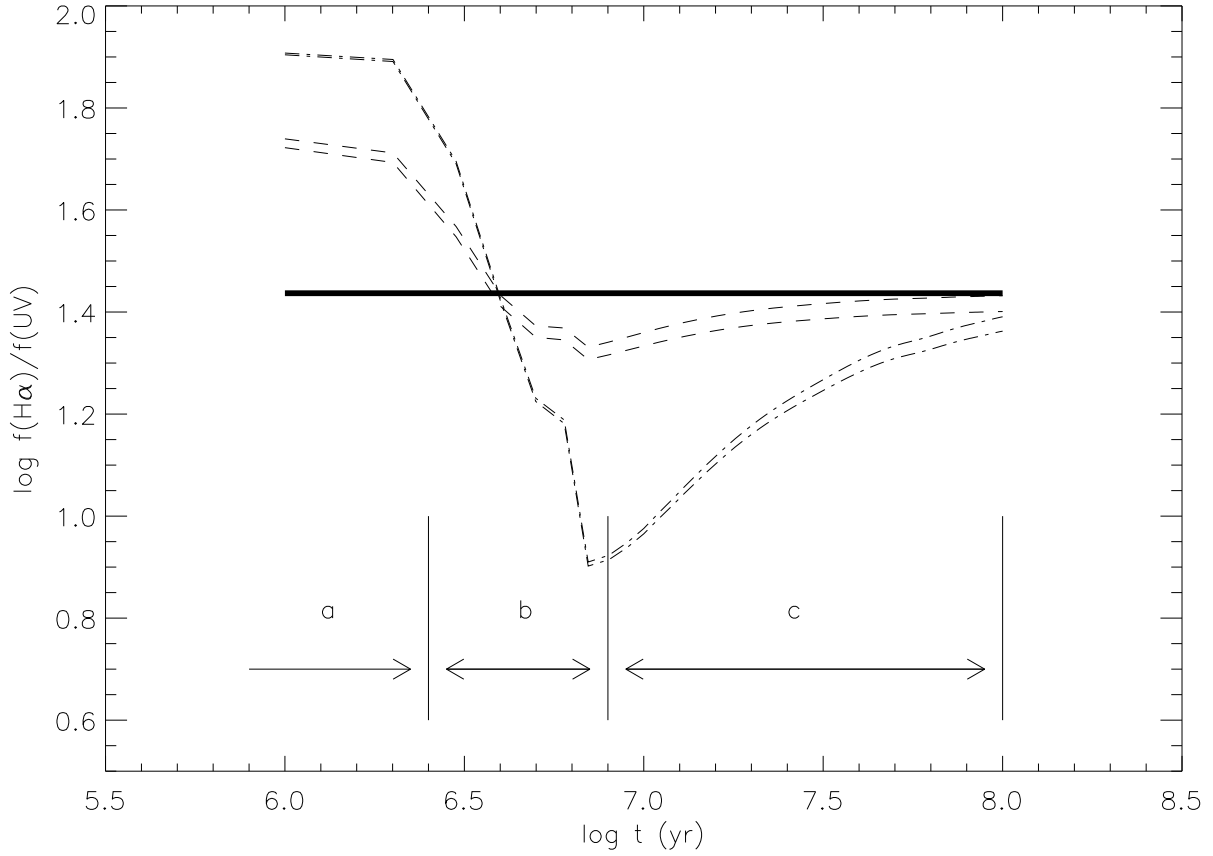


Fig. 4. Effect of instantaneous bursts of star formation on the $f(\text{H}\alpha)/f(\text{UV})$ ratio over a normal evolution “a la Sandage”. The thick continuous line represents unperturbed evolution “a la Sandage” for $3.2 \leq \tau \leq 15$ Gyr (the thickness of the line accounts for the dispersion of the models). The Salpeter IMF and solar metallicity are assumed. The X axis gives the age of the instantaneous burst, assuming galaxies 13 Gyr old. The dashed (dot dashed) lines correspond to star formation bursts of intensities 10 (100) times the corresponding “a la Sandage” SFR at $t = 13$ Gyr for $\tau = 3.2$ and 15 Gyr.

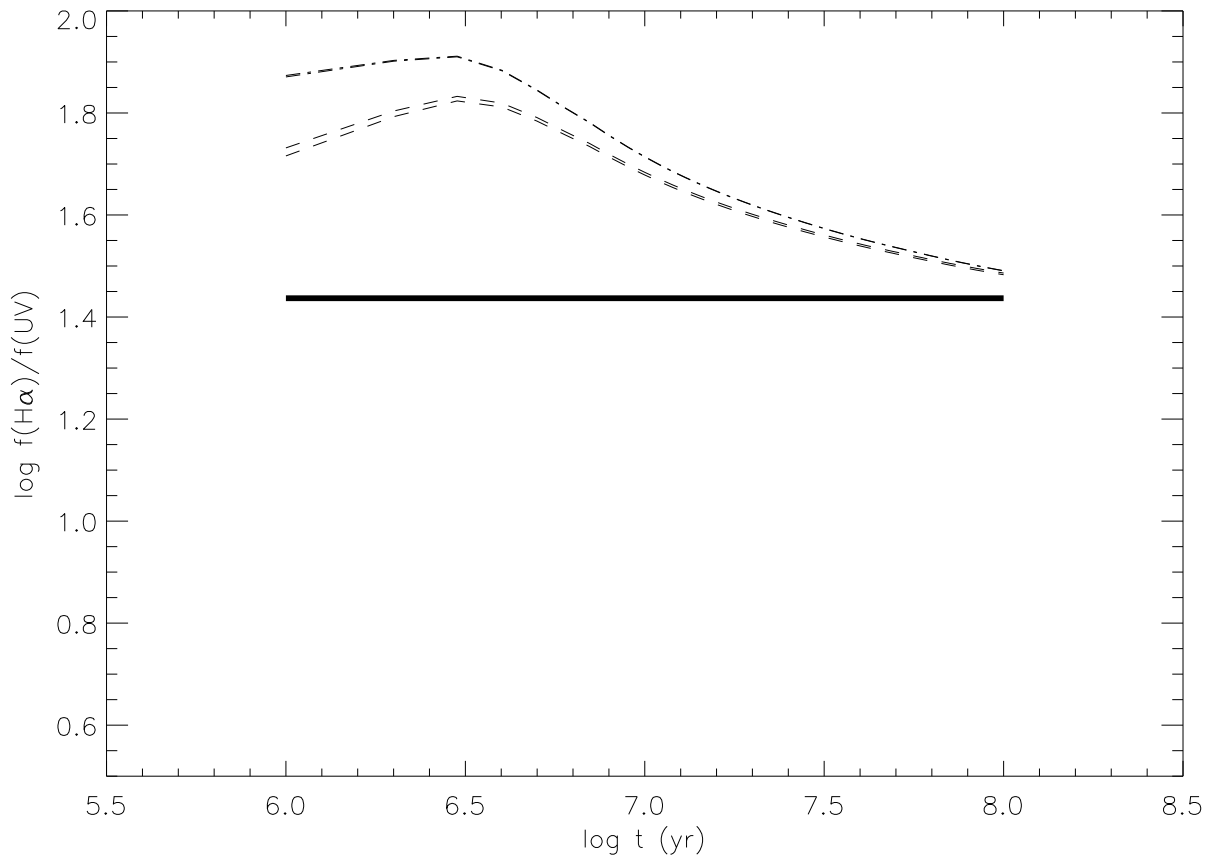


Fig. 5. Same as fig. 4 for a burst of 10^8 yr duration.

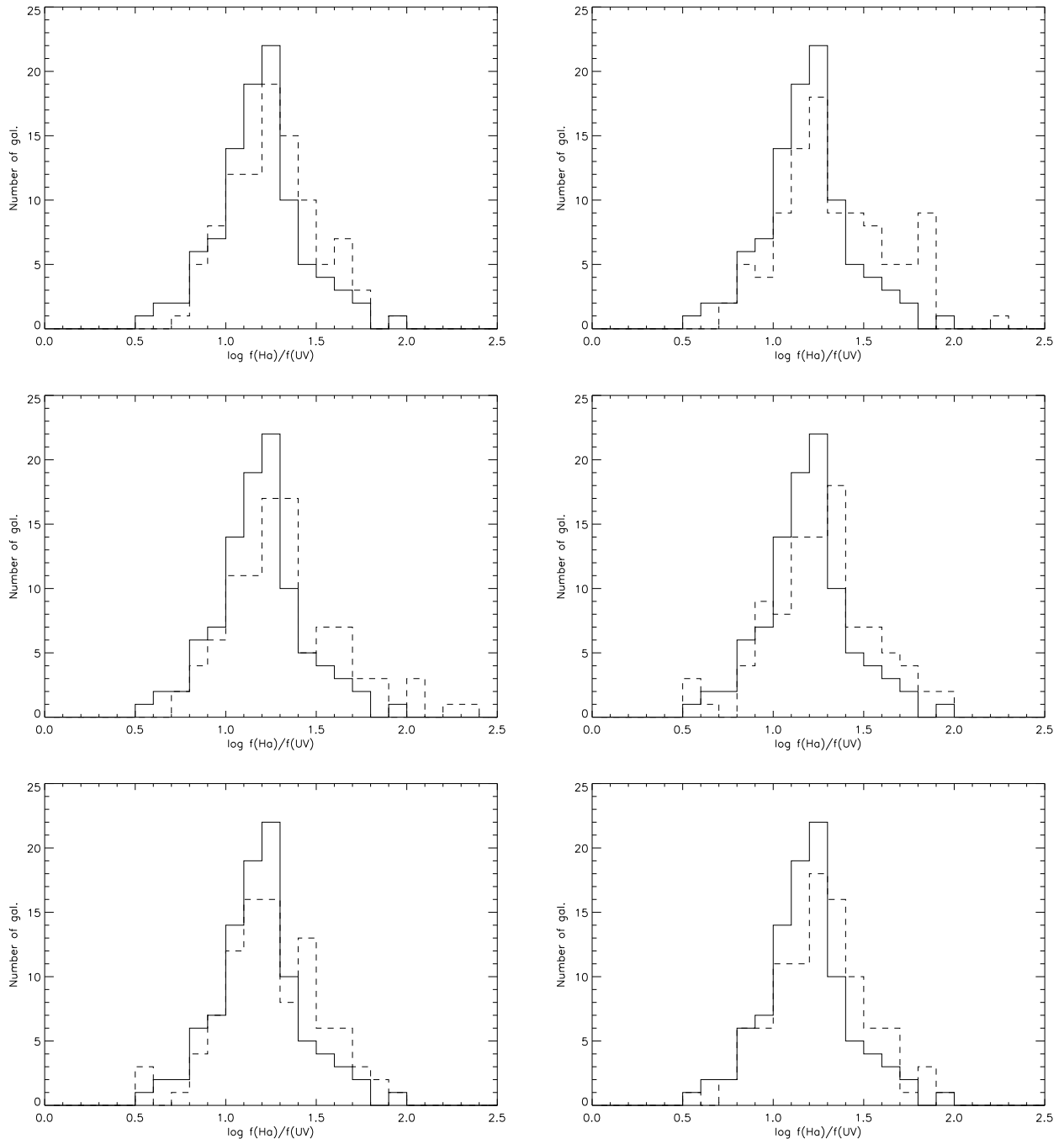


Fig. 6. Histograms of $f(\text{H}\alpha)/f(\text{UV})$ for six different simulations of scenarios 9 and 12 (dashed lines). The observed histogram is given with solid lines.

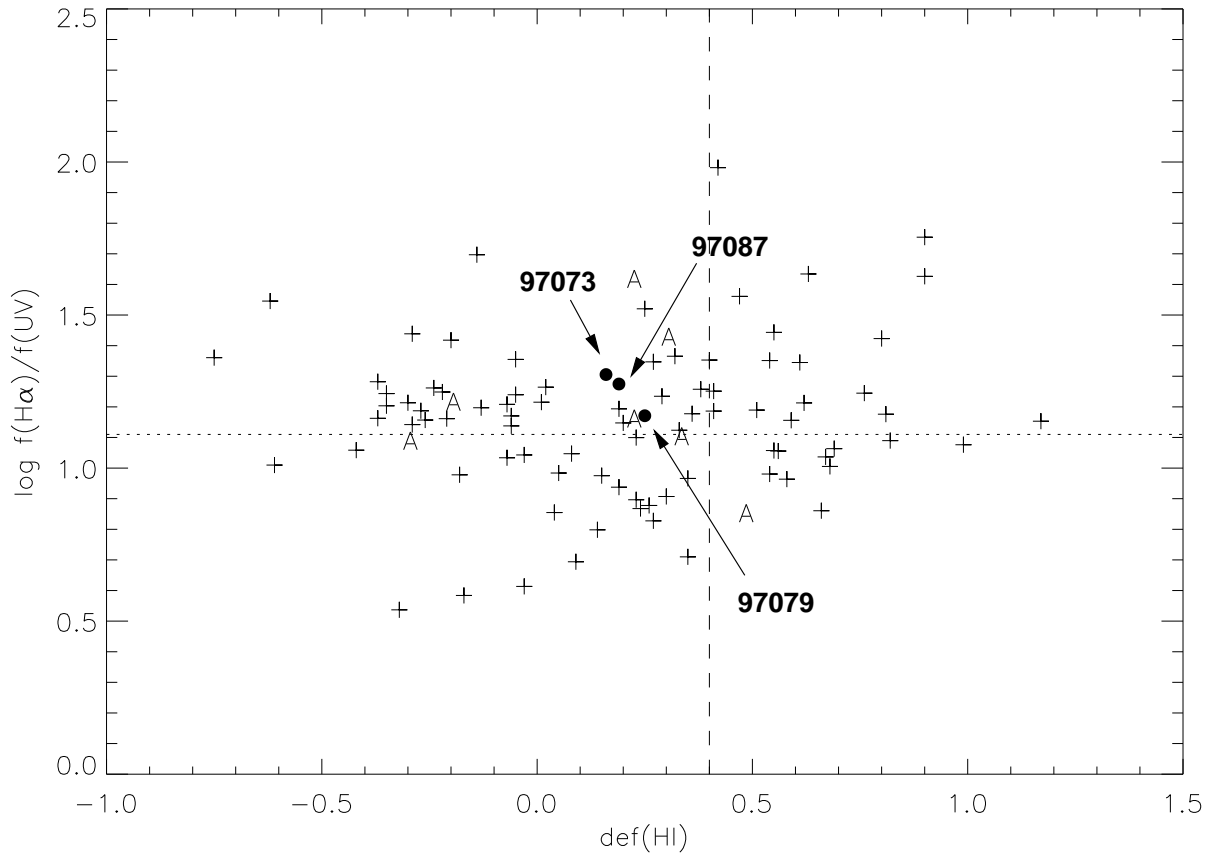


Fig. 7. The relationship between $\log f(H\alpha)/f(UV)$ and the HI deficiency. Interacting galaxies are marked with filled dots. Galaxies with asymmetric HI profiles are labeled with “A”. The short-dashed horizontal line corresponds to the average value of $f(H\alpha)/f(UV)$ for the reference sample. The dashed vertical line corresponds to $def(HI) = 0.4$: pluses with $def(HI) \leq 0.4$ represent the reference sample.

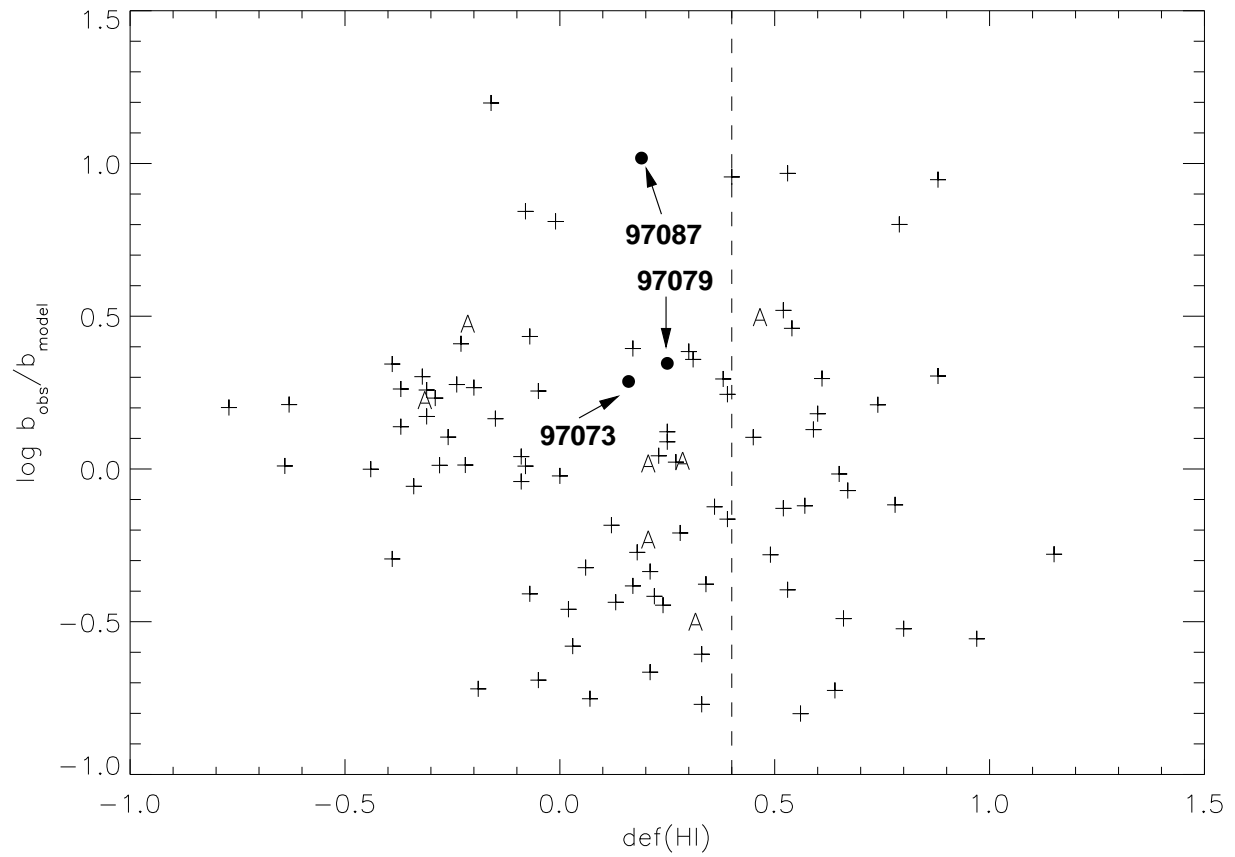


Fig. 8. The relationship between $\log b_{\text{obs}}/b_{\text{model}}$ and the HI deficiency. The dashed vertical line corresponds to $\text{def}(\text{HI}) = 0.4$. Symbols as in fig. 7.

Appendix A: The intensity of the star formation bursts

The b parameter is the ratio of the recent to the total SFRs over the whole life of a galaxy as defined by Kennicutt et al. (1994). If the SFR of a galaxy as a function of time is known, then:

$$b = \frac{\text{SFR}(t, \tau) \times t}{\int_0^t \text{SFR}(t', \tau) dt'} \quad (\text{A.1})$$

where t is the current epoch and the galaxies are assumed to be formed at $t' = 0$. If a simple exponential SF history is assumed:

$$\text{SFR}(t, \tau) = \text{SFR}_0 e^{-t/\tau} \quad (\text{A.2})$$

the b parameter can be expressed, following Boselli et al. (2001) as:

$$b_{\text{model}} = \frac{t \times e^{-t/\tau}}{\tau(1 - e^{-t/\tau})} \quad (\text{A.3})$$

These authors also report an empirical relationship:

$$\log L_{\text{H}} = -2.5 \times \log \tau + 12 \quad (\text{A.4})$$

that, together with eq. A.3, provides the link between the b parameter and the H -band luminosity of a galaxy, in the case of an exponential SFH of eq. A.2.

An independent way to obtain the value of b from purely observational considerations is as following Boselli et al. (2001):

$$b_{\text{obs}} = \left(\frac{L_{\text{H}\alpha}}{10^{41}} \right) \times 0.26 \times \left(\frac{t}{L_{\text{H}}} \right) \quad (\text{A.5})$$

where t is as in eq. A.1 in yr, and $L_{\text{H}\alpha}$ and L_{H} are the H α and H -band luminosities respectively.

The comparison of b obtained from the average empirical relationship between τ and L_{H} (i.e. b_{model}), and from L_{H} and $L_{\text{H}\alpha}$ (i.e. b_{obs}) should reflect the deviations from a smooth evolution on timescales of the order of 3×10^6 yr.

Appendix B: The error budget

This appendix is aimed at estimating the total error budget of the $f(\text{H}\alpha)/f(\text{UV})$ ratio as computed from our data. We adopt the following expression for the $f(\text{H}\alpha)/f(\text{UV})$ ratio:

$$\begin{aligned} \log f(\text{H}\alpha)/f(\text{UV}) = & \log f_0(\text{H}\alpha) \pm \Delta f_0(\text{H}\alpha) - \log \left[1 + \frac{I(\text{H}\alpha)}{I([\text{NII}])} \times \frac{1 \pm \Delta I(\text{H}\alpha)}{1 \pm \Delta I([\text{NII}])} \right] - \left(\frac{1}{0.335} - 1 \right) \times \\ & \times \log \left[\frac{I(\text{H}\alpha)}{I(\text{H}\beta)} \frac{1}{2.87} \times \frac{1 \pm \Delta I(\text{H}\alpha)}{1 \pm \Delta I(\text{H}\beta_{\text{emi}} \pm \Delta I(\text{H}\beta_{\text{abs}}))} \right] - \log f_0(\text{UV}) \pm \Delta f_0(\text{UV}) - \\ & - 0.466 - \log \left[\frac{f_0(\text{Far-IR})}{f_0(\text{UV})} \times \frac{1 \pm \Delta f_0(\text{Far-IR})}{1 \pm \Delta f_0(\text{UV})} \right] - 0.433 \times \log \left[\frac{f_0(\text{Far-IR})}{f_0(\text{UV})} \times \frac{1 \pm \Delta f_0(\text{Far-IR})}{1 \pm \Delta f_0(\text{UV})} \right]^2 \end{aligned} \quad (\text{B.1})$$

where,

- $f_0(\text{H}\alpha)$, $f(\text{Far-IR})$ and $f_0(\text{UV})$ are the measured integrated luminosities from imaging data in the corresponding passbands,
- $\Delta f_0(\text{H}\alpha)$, $\Delta f_0(\text{Far-IR})$ and $\Delta f_0(\text{UV})$ are the uncertainties of the H α , Far-IR and UV fluxes,
- $I(\text{H}\alpha)$, $I(\text{H}\beta)$ and $I([\text{NII}])$ are the fluxes of the corresponding emission lines as measured from the optical spectra,
- $\Delta I(\text{H}\alpha)$, $\Delta I(\text{H}\beta_{\text{emi}})$ and $\Delta I([\text{NII}])$ are the uncertainties on the fluxes of the corresponding emission lines,
- $\Delta I(\text{H}\beta_{\text{abs}})$ is the uncertainty on the flux of the H β absorption line.

The formula used to derive the extinction at 2000 Å was taken from Buat et al. (1999). In order to estimate our total error budget, we run Monte-Carlo simulations of the distribution of 56 values with the error budget shown in eq. B.1. The individual sources of uncertainty were assumed to follow a gaussian distribution. The error sources are listed in Table B.1. For our simulations we assumed typical values of $f_0(\text{Far-IR})/f_0(\text{UV}) = 1$, $I(\text{H}\alpha)/I(\text{H}\beta) = 3$ and $I([\text{NII}])/I(\text{H}\alpha) = 0.2$. The simulated distributions turned out to be fairly symmetric with typical dispersions of $\sigma = 0.27 \pm 0.03$ dex. The centers of the distributions showed typical variations of ± 0.03 dex.

Table B.1. The error sources entering the computation of the uncertainty in the $f(\text{H}\alpha)/f(\text{UV})$ ratio.

Uncertainty source	Estimated
$\Delta f_0(\text{H}\alpha)$	15%
$\Delta f_0(\text{Far-IR})$	15%
$\Delta f_0(\text{UV})$	20%
$\Delta I(\text{H}\alpha)$	10%
$\Delta I(\text{H}\beta_{\text{emi}})$	10%
$\Delta I(\text{N}[\text{II}])$	15%
$\Delta I(\text{H}\beta_{\text{abs}})$	20%